Analytica Chimica Acta: X 1 (2019) 100004

Contents lists available at ScienceDirect

Analytica Chimica Acta: X

journal homepage: www.journals.elsevier.com/analytica-chimica-acta-x

On the mechanism of protein supercharging in electrospray ionisation mass spectrometry: Effects on charging of additives with short- and long-chain alkyl constituents with carbonate and sulphite terminal groups

Eric D.B. Foley [a, 1], Muhammad A. Zenaidee [a], Rico F. Tabor [b], Junming Ho [a], Jonathon E. Beves [a], William A. Donald [a, *]

[a] School of Chemistry, University of New South Wales, Sydney, NSW, Australia, 2052
[b] School of Chemistry, Monash University, Melbourne, VIC, Australia, 3800

ARTICLE INFO

Article history:
Received 5 September 2018
Received in revised form
16 November 2018
Accepted 21 December 2018
Available online 28 December 2018

Keywords:
Electrospray ionisation
Mass spectrometry
Protein ions
Supercharging
Ion evaporation model
Charge residue model
Chain ejection model
1,2-butylene carbonate
1,2-hexylene carbonate
1,2-propylene carbonate

ABSTRACT

Small organic molecules are used as solution additives in electrospray ionisation mass spectrometry (ESI-MS) to increase the charge states of protein ions and improve the performance of intact protein analysis by tandem mass spectrometry. The properties of the additives that are responsible for their charge-enhancing effects (*e.g.* dipole moment, gas-phase basicity, Brønsted basicity, and surface tension) have been debated in the literature. We report a series of solution additives for ESI-MS based on cyclic alkyl carbonates and sulphites that have alkyl chains that are from two to ten methylene units long. The extent of charging of [Val [5]]-angiotensin II, cytochrome *c*, carbonic anhydrase II, and bovine serum albumin in ESI-MS using the additives was measured. For both the alkyl carbonate and sulphite additives with up to four methylene units, ion charging increased as the side chain lengths of the additives increased. At a critical alkyl chain length of four methylene units, protein ion charge states decreased as the chain length increased. The dipole moments, gas-phase basicity values, and Brønsted basicities (*i.e.* the pK_a of the conjugate acids) of the additives were obtained using electronic structure calculations, and the surface tensions were measured by pendant drop tensiometry. Because the dipole moments, gas-phase basicities, and pK_a values of the additives did not depend significantly on the alkyl chain lengths of the additives and the extent of charging depended strongly on the chain lengths, these data indicate that these three additive properties do not correlate with protein charging under these conditions. For the additives with alkyl chains at or above the critical length, the surface tension of the additives decreased as the length of the side chain decreased, which correlated well with the decrease in protein charging. These data are consistent with protein charging being limited by droplet surface tension below a threshold surface tension for these additives. For additives with relatively high surface tensions, protein ion charging increased as the amphiphilicity of the additives increased (and surface tension decreased) which is consistent with protein charging being limited by the emission of charge carriers from highly charged ESI generated droplets.
© 2018 Published by Elsevier B.V. This is an open access article under the CC BY-NC-ND license (http://creativecommons.org/licenses/by-nc-nd/4.0/).

1. Introduction

Electrospray ionisation (ESI) [1–3] can be used to form intact protein ions in the gas phase in higher charge states than any other known technique. Forming highly charged analyte ions lowers their mass-to-charge ratio (m/z) and enables mass analysers with limited mass ranges to detect analyte ions as large as proteins [2]. Moreover, protein ions in higher charge states generally dissociate more extensively than ions in lower charge states in widely-used ion

* Corresponding author. UNSW Sydney School of Chemistry Dalton Building, Room 221 Kensington, NSW, 2052, Australia.
E-mail address: w.donald@unsw.edu.au (W.A. Donald).
[1] Current address: EPSRC & MRC Centre for Doctoral Training in Biomedical Imaging, University of Oxford, Oxford, United Kingdom, OX1 3QU.

https://doi.org/10.1016/j.acax.2018.100004
2590-1346/© 2018 Published by Elsevier B.V. This is an open access article under the CC BY-NC-ND license (http://creativecommons.org/licenses/by-nc-nd/4.0/).

fragmentation techniques such as collision induced dissociation (CID), electron transfer dissociation (ETD), and electron capture dissociation (ECD) [4–6]. During ECD and ETD (ExD), post-translational modifications of proteins and peptides tend to remain intact [6–8], which can be a significant advantage over other fragmentation methods, including CID [9]. In ExD, the charge sites direct fragmentation [8,10–13] and the energy deposited into the ion increases with charge state [10,11,14–18]. As such, high peptide and protein charge states result in high fragmentation efficiencies and extensive ion fragmentation. However, it remains challenging to obtain extensive fragmentation of protein ions larger than 20 kDa owing partly to the strength of intramolecular non-covalent interactions [6,11,13,19]. To overcome the non-covalent forces of large protein ions, denaturing electrospray solutions, which are used to form protein ions in extremely high charge states and unfolded conformations [6,20–24], can be employed. Thus, the ability to form protein ions in unfolded conformations and higher charge states than is currently possible should result in further improvements to the fragmentation efficiency of large protein ions in ExD.

In ESI, an electrical potential is applied to a solution flowing through a capillary, which results in the formation of a plume of highly charged droplets that contain analytes [1–3]. The components of the droplets evaporate at rates in order of decreasing volatility, which results in smaller droplets [25]. When the droplets reach a critical size, Coulombic repulsion overcomes the surface tension of the droplets and results in Coulombic fission; *i.e.* a stream of smaller droplets is emitted [1–3]. For a spherical droplet holding a given amount of charge, the critical droplet radius at which droplet fission occurs is given by the Rayleigh limit [26].

$$Q_{CF} = 8\pi\left(\gamma\varepsilon_0 R^3\right)^{\frac{1}{2}} \quad (1)$$

where Q_{CF} is the charge on the droplet, γ the surface tension of the droplet, R the radius of the droplet, and ε_0 the electrical permittivity of vacuum. Repeated droplet fission results in highly charged nanodroplets from which the protein ions are ultimately formed. As Coulombic fission causes the total charge in the precursor droplets to decrease [27], the amount of charge in the nanodroplets in the final stages of ESI will depend on the frequency of Coulombic fission events. Additionally, droplets can lose charge due to the emission of charge carriers from the nanodroplets in a process called ion emission [28]. Thus, it is desirable to minimise both Coulombic fission and ion emission events to maximise the amount of charge in the nanodroplets near the moment of protein ion formation.

The charge states of protein ions formed by ESI can be significantly increased by adding superchargers (*e.g.* *m*-NBA [29], sulfolane [30], propylene carbonate [31], and butylene carbonate [32]) to electrospray solutions [30,33–37]. For example, by using a denaturing solution consisting of 94.5%(v/v) water, 0.5%(v/v) acetic acid, and 5% (v/v) butylene carbonate, ESI can be used to form common test protein ions in higher charge states than has been reported by use of denaturing acidic aqueous solutions containing high concentrations of organic solvent, or by the use of other supercharging additives; that is, doping butylene carbonate into a denaturing solution can increase the average charge states of myoglobin from 20.6 ± 0.5 to 30.6 ± 0.2, respectively [32]. Furthermore, the use of 1,2-butylene carbonate resulted in the identification of cleavage sites at more than 85% of all inter-residue bonds in the ECD mass spectra of single charge states of protein ions with masses up to 66.5 kDa [6].

The mechanism of forming supercharged protein ions from denatured ESI solutions has been actively debated in the literature [38]. Superchargers are significantly less volatile than other ESI solution components (*e.g.* water and methanol), which results in the enrichment of such additives in the droplets during the ESI process [25,31,34,39,40]. In the dipole moment model, the relatively high electric dipole moments of supercharging additives may decrease the Coulombic repulsion inside the ESI droplets to increase the extent of charge that ESI generated droplets can accomodate [41]. More highly charged droplets should form more highly charged analyte ions. In the Brønsted basicity model, the ability of additives to increase the charge on analyte ions is inversely related to the Brønsted basicities of the additives in water (*i.e.* more negative pK_a values of the conjugate acids of the additives in water can result in the formation of higher protein charge states) [40]. The gas-phase basicities of solution additives and solvent molecules from the ESI source have also been implicated in limiting the extent of protein ion charging owing to proton-transfer reactions [42]. In the surface tension model [29], the supercharging effect results from the relatively high surface tension of solution additives (>38 mN m^{-1}) that can result in increased analyte charging. Generally, the least volatile component in denaturing ESI solutions is acetic acid ($\gamma = 27.12$ mN m^{-1}) [43]. The initial ESI droplets can consist of a large fraction of water ($\gamma = 72.01$ mN m^{-1}) [43] and thus possess relatively high surface tensions. For binary water-acetic acid mixtures, water evaporates more rapidly than acetic acid [44]. Thus, the nanodroplets in the final stages of ESI are likely to be enriched with acetic acid and thus should have lower surface tensions than pure water [44]. The addition of molecules with lower volatility and larger surface tensions than acetic acid or acetic acid/water mixtures should result in an increase of the surface tension of the ESI nanodroplets near the moment of ion formation. Based on the Rayleigh limit (Equation (1)), increasing the surface tension of the nanodroplets should result in the accommodation of more charge per droplet prior to fission, and ultimately the release of more highly charged protein ions.

To date, several studies have been conducted to elucidate the mechanism of protein charging and supercharging in ESI, some of which have raised questions about the impact of the dipole moment [31], the gas-phase basicity [32,45,46], Brønsted basicity [32], and the surface tension [32,34,47] of superchargers on the extent of protein charging. For example, the average charge state of cytochrome *c* increased from 21.5 ± 0.2 to 22.6 ± 0.2 as the alkyl chain length of cyclic alkyl carbonate additives increased from ethylene carbonate to 1,2-butylene carbonate [32]. However, the surface tension decreases from ethylene carbonate (54.6 mN m^{-1}) [48] to 1,2-butylene carbonate (38.0 mN m^{-1}), which in the absence of other factors is inconsistent with predictions based solely on Equation (1). Moreover, the increase in the charge states of the protein ions observed as the alkyl chain length of the cyclic alkyl carbonates increases suggests that the amphiphilicity of the supercharging additives may play a role in the extent of protein ion charging. Recently, Konermann and co-workers proposed that superchargers in “native” ESI solutions reside at the surface of the ESI nanodroplets and can interfere with charge carriers exiting the nanodroplets [49]. This ‘charge-trapping model’ was supported by molecular dynamics simulations and complementary experimental data [49]. In this model, the amphiphilicity of supercharging additives should affect the extent of protein charging.

The supercharging additives that have been reported to date generally have multiple physicochemical properties that differ significantly; that is, many properties can be changed by testing each additive. For example, additives that have been compared for their effectiveness in increasing analyte charging can have gas-phase basicity values, dipole moments, and surface tensions that differ by over 100 kJ mol^{-1}, 3 D, and 30 mN m^{-1}, respectively [29,31]. Moreover, the Brønsted basicities of some supercharging additives in water have not been reported [31,32,40]. As such, it remains challenging to precisely and accurately identify the

properties of these molecules that are responsible for their charge-enhancing effects, which may partially contribute to the controversy regarding the proposed mechanisms and conflicting experimental evidence. These circumstances prompted us to determine the effects of more 'subtly' and systematically investigating the properties of superchargers on the extent of protein charging in ESI-MS. We selected a series of cyclic alkyl carbonates and cyclic alkyl sulphites (Fig. 1) with different alkyl chain lengths as ESI additives, such that: (i) the dipole moments, gas-phase basicity values, and Brønsted basicities should remain relatively constant because these properties should be strongly influenced by the polar head groups and should not depend significantly on the alkyl chain length, and (ii) the surface tensions should significantly decrease as the lengths of the alkyl chains increase. The additives that were not readily available from commercial sources were synthesised (**C3-C8**; **S0-S8**; Fig. 1). By comparing the extent of protein ion charging that is obtained using the solution additives **C0-C8** and **S0-S8** (Fig. 1) in ESI-MS experiments to the physicochemical properties of these additives, the effects of surface tension on the extent of protein charging in ESI can be more readily elucidated.

2. Materials and methods

2.1. General methods

NMR spectra were recorded at 298 K on a Bruker Avance III 400 MHz spectrometer. The chemical shifts for ^{1}H NMR spectra are given with reference to residual solvent resonance. High resolution mass spectrometry (HR-MS) data for the synthesised molecules were collected using a hybrid linear quadrupole ion trap mass spectrometer coupled to a 7 T Fourier transform ion cyclotron resonance mass spectrometer (LTQ/FT-ICR, Thermo Scientific). Liquid density measurements were performed in triplicate at 25.0 °C for 1.5 mL solutions on an Anton Paar Density Meter DMA 4100 M. Surface tension values were measured using a custom pendant drop tensiometer at Monash University [50]. Pendant drop tensiometry can be used to accurately determine the surface tensions of a variety of liquids to within 0.1–0.2 mN m^{-1} [50]. In this study, surface tensions were reproducible to within 0.2–0.8 mN m^{-1}. For full details on the surface tension measurements, refer to the Supplementary Information (Fig. S1 and Table S1). Circular dichroism experiments were performed on a Chirascan Plus spectrometer (Applied Photophysics) using the instrument parameters recommended by the manufacturer (1 nm bandwidth, 0.5 cm increments, 0.1 mm pathlength, 3 s for each data point, and N_2 flow of 5 L min^{-1}). The spectra were acquired from 185 to 240 nm (see Supplementary Information Fig. S2).

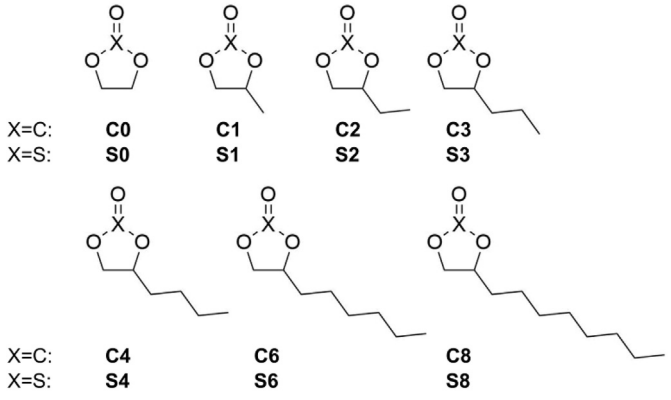

Fig. 1. Compounds selected for use as solution additives in electrospray ionisation mass spectrometry experiments.

2.2. Mass spectrometry experiments

All ESI-MS experiments were conducted using a LTQ/FT-ICR MS (Thermo Scientific) equipped with an external ESI source. Analyte solutions were infused into the ESI source at 3 μL min^{-1} flow rates (500 μL gas tight syringe, Hamilton 1700 Series) and a voltage of 3.5–5.0 kV was applied between the ESI capillary and the capillary entrance to the MS to form ions. LTQ-MS ion optic parameters were optimised to obtain stable and intense protein ion signal and to maximise the abundance of the highest protein ion charge states. For comparing the supercharging effects of different additives, the same ion optic parameters were used for all samples, and the mass spectra were collected using the LTQ-MS. Protein solutions were prepared from aqueous stock solutions (100 μM) that were stored at 4 °C for a maximum of three days. ESI solutions consisted of a constant solvent matrix (~80/19/1% v/v methanol/water/acetic acid), 1–6% of the solution additive of interest, and 5–10 μM of a peptide or protein, specifically 10 μM cytochrome *c*, 10 μM [Val [5]]-Angiotensin II acetate, 5 μM carbonic anhydrase II, and 5 μM bovine serum albumin. For ESI-MS, the synthesised additives were isolated and purified, without the separation of any diastereomers or enantiomers. For assignment of the diastereomers of **S1-S8**, please refer to the Supplementary Information and Fig. S3.

2.3. Materials

Cytochrome *c* (equine heart; 12 kDa) was obtained from Alfa Aesar. Carbonic anhydrase II (bovine erythrocytes: 29 kDa), bovine serum albumin (66 kDa), and [Val [5]]-Angiotensin II acetate (1032 Da) were obtained from Sigma Aldrich. Methanol (99.7%) and acetic acid (99.7%) were purchased from Ajax Finechem. Water was obtained from a Milli-Q water purification system with a resistance of at least 18 Ω. Ethylene carbonate (**C0**) and propylene carbonate (**C1**) were obtained from Sigma Aldrich, and 1,2-butylene carbonate (**C2**) was obtained from Tokyo Chemical Industries. All starting materials for synthetic procedures were purchased from commercial sources and used without further purification.

2.4. Data analysis

Mass spectra were collected in quadruplicate and processed using XCalibur™ (Thermo Scientific) and the average protein charge states (<*z*>) were calculated using Equation (2):

$$<z> = \frac{\Sigma(zI_z)}{\Sigma I_z} \quad (2)$$

where I_z is the integrated abundance of each charge state (*z*). The precision of the average charge states was obtained from the standard deviations of the replicate mass spectra.

2.5. Computational calculations

Computational calculations for the dipole moments were performed using TPSS/aug-cc-pVDZ//TPSS/aug-cc-pVDZ for **C0-C8** and B3LYP/6–311++G(2d,p)//B3LYP/6–311++G(2d,p) for **S0-S8**. The gas-phase basicity values were calculated using B3LYP/6–311++G(2d,p)//B3LYP/6–311++G(2d,p) and G3(MP2)-CC [51]//M06–2X/6-31G(d) [52] for both **C0-C8** and **S0-S8**. These method-basis set combinations were selected based on benchmarking results that are reported in the Supplementary Information (Figs. S4–5 and Tables S2–5). All calculations were performed using Gaussian 09 (revision B01) [53] and Gaussian 16 (revision A03) [54]. Calculations were carried out for the major conformers of each molecule and the results for gas-phase basicity values and dipole

moments were weighted by the Boltzmann populations of the major conformers. For additives **S1**-**S8** the calculated properties were averaged using the diastereomeric excess measured by ^{1}H NMR (Fig. S3).

Electronic structure calculations to determine the solution-phase pK_a values (in water) of the conjugate acids of **C0**-**C8** and **S0**-**S8** were carried out using the Gaussian16 (revision A03) [54], Q-CHEM [55], and NWCHEM [56] programs and a combination of G3(MP2)-CC [51]//M06−2X/6-31G(d) [52] and the SM8 [57] solvation model (Supplementary Information and Table S6). For the proton, we used the gas-phase free energy of −26.3 kJ mol^{-1} [58], and a fixed concentration solvation free energy of −1112.5 kJ mol^{-1} [59,60]. Both absolute and relative pK_a calculation schemes were considered [61,62]. As informed by a previous study [63], the proton solvation free energy has a relatively large uncertainty of at least 10 kJ mol^{-1} which may be even larger [64–66] and translates to an error of 2 or more pK_a units. For this reason, we report both absolute and relative pK_a values. For full details on the computational calculations and conformational analysis refer to the Supplementary Information and Fig. S6.

2.6. Synthetic procedures

Additives **C3**-**C8** and **S0**-**S8** were synthesised following modified literature procedures [67,68]. They were then purified using column chromatography and their chemical structure was confirmed using ^{1}H NMR spectroscopy and high-resolution mass spectrometry (>97% purity as determined by ^{1}H NMR). For further details, refer to the Supplementary Information.

3. Results and discussion

3.1. Effect of solution additives on protein charge states

Representative ESI mass spectra of 10 μM cytochrome *c* in denaturing solutions doped with 'optimal' amounts of **C2** (2%), **S2** (5%), and **C6** (3%) are shown in Fig. 2; *i.e.* these concentrations resulted in the formation of protein ions in the highest average charge states without detrimentally affecting the ion signal under these conditions. The more hydrophobic additives (*e.g.* **S8** and **C8**) did not readily dissolve in aqueous matrices, so a mixture of ~80/19/1% v/v methanol/water/acetic acid was chosen as the solution composition for all ESI-MS experiments; *i.e.* this composition contained the minimum amount of methanol necessary to dissolve all cyclic alkyl carbonate and sulphite additives at concentrations up to 5% v/v. The extent of protein charging in ESI-MS depended strongly on the identity of the solution additives. For example, the addition of 2% **C2** to denaturing solutions (~80/19/1% v/v methanol/water/acetic acid) containing 10 μM cytochrome *c* (cyt *c*) resulted in an increase in the average charge state (<*z*>) of cyt *c* from 14.7 ± 0.1 to 20.5 ± 0.1, an increase in the most abundant charge state from 15 to 22, and an increase in the highest observed charge state from 20 to 22. In contrast, the use of 5% **S2** resulted in an average charge state for cyt *c* of 18.3 ± 0.1, a most abundant charge state of 20, and a highest observed charge state of 23 (Fig. 2). The addition of **C6** resulted in a significant broadening of the charge state distribution of cyt *c*, and a lower <*z*> value than that obtained without any additive (14.4 ± 0.1 and 14.7 ± 0.1, respectively). Similar trends were observed with carbonic anhydrase II (CAII), although being a larger protein, CAII (29 kDa) ions were formed in higher charge states than cyt *c* (12 kDa).

To investigate the effect of the additive chain length on the extent of protein and peptide charging, **C0**-**C8** and **S0**-**S8** were added to ESI solutions containing cytochrome *c* (cyt *c*; 12 kDa), carbonic anhydrase II (CAII; 29 kDa) [Val [5]],-Angiotensin II acetate (AngII; 1032 Da), and bovine serum albumin (BSA; 66 kDa). The solution additives were doped into the ESI solutions at their 'optimal' concentrations (Table 1). Full details regarding the optimisation of the additive concentrations are given in the Supplementary Information (Fig. S7). The average charge states of CAII, cyt

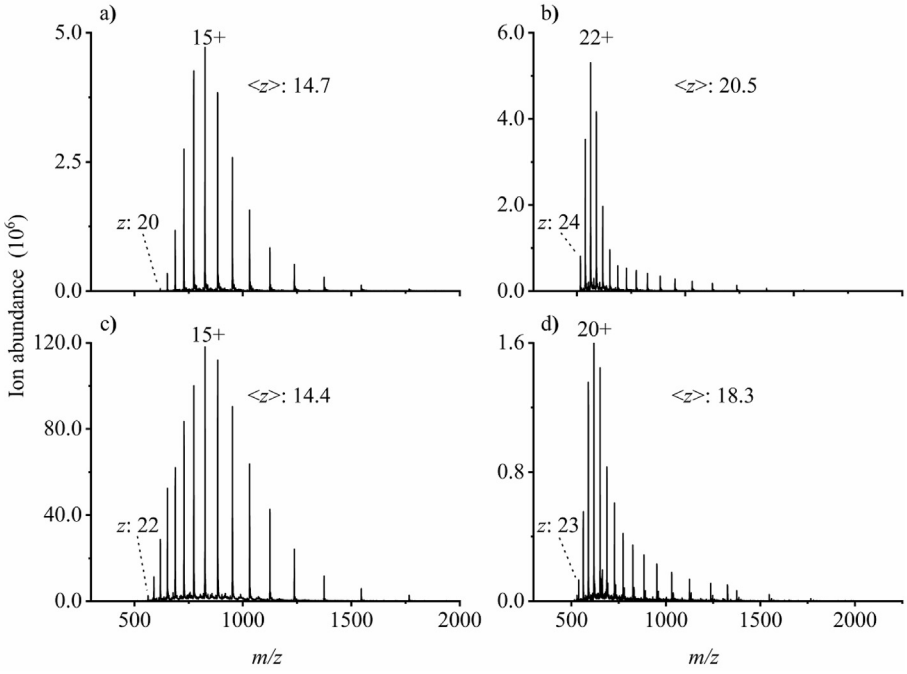

Fig. 2. ESI mass spectra of denaturing solutions (~80/19/1% methanol/water/acetic acid) containing cytochrome *c* obtained using a) no additive, and an 'optimal' amount of b) **C2** (~2%), c) **C6** (~3%), and d) **S2** (~5%). The most abundant charge state, the highest observed charge state (*z*), and the average charge state (<*z*>) of cytochrome *c* are displayed on each spectrum.

Table 1
Optimal concentrations of the selected solution additives in denaturing solutions for maximising the extent of protein ion charging in ESI-MS. Refer to Fig. S7 in the Supplementary Information for details.

Carbonate additive	Optimal conc. (% v/v)	Sulphite additive	Optimal conc. (% v/v)
C0	2	S0	4
C1	2	S1	5
C2	2	S2	5
C3	3	S3	4
C4	4	S4	4
C6	3	S6	4
C8	3	S8	4

c, AngII, and BSA obtained with additives **C0-C8** and **S0-S8** are presented in Fig. 3. For tabulated data please refer to Table S7 in the Supplementary Information.

Generally, the use of the cyclic alkyl sulphites resulted in lower average charge states for AngII, cyt *c*, and CAII than the use of the cyclic alkyl carbonates with the same alkyl chain lengths. Out of all tested solution additives, the use of **C2** resulted in the highest average charge states for AngII (2.49 ± 0.01), cyt *c* (20.5 ± 0.1), CAII (36.3 ± 0.1), and BSA (64.7 ± 0.1), whereas some additives resulted in average charge states as low or lower than those obtained in the absence of any additives (*e.g.* **C8** and **S8**). The average charge states of all four analytes increased from **C0** to **C2** and from **S0** to **S2** and then decreased from **C2** to **C8** and from **S2** to **S8** as the alkyl chain lengths increased, which suggests that the trends in protein charge states with increasing chain lengths of the additives is a general phenomenon.

3.2. Effects of dipole moment, gas-phase basicity, Brønsted basicity, and surface tension on the extent of protein charging

To rationalise the effects of the additives on the extent of protein ion charging (Fig. 3), we investigated the key physicochemical properties of the additives that have been implicated in impacting protein charging in ESI in the literature (*e.g.* dipole moment, gas-phase basicity, Brønsted basicity, surface tension, and the effects of **C0-C8** on protein structures in solution). For **C0-C8** and **S0-S8**, the measured values for the dipole moments, gas-phase basicities and solution-phase pK_a values of their conjugate acids (Brønsted basicity) are either not available in the literature, or only exist for the smallest additives. Rowley and co-workers demonstrated that *ab initio* quantum chemistry methods can calculate the electric dipole moments of over 40 molecules to within 0.1 D [69]. Similarly, *ab initio* and composite methods have been used to calculate the gas-phase basicity [70,71] and pK_a values in aqueous solution [61,62] of several organic molecules with reasonable accuracy.

Based on the results obtained from benchmarking calculations (Supplementary Information Figs. S4–5 and Tables S2–5), we selected TPSS/aug-cc-pVDZ and B3LYP/6−311++G(2d,p) for the calculation of the dipole moments of additives **C0-C8** and **S0-S8**, respectively (Tables S8–9). The gas-phase basicity values of additives **C0-C8** and **S0-S8** were calculated using B3LYP/6−311++G(2d,p) and G3(MP2)-CC//M06−2X/6-31G(d), however, the gas-phase basicity values for **C0-C8** and **S0-S8** only differed by

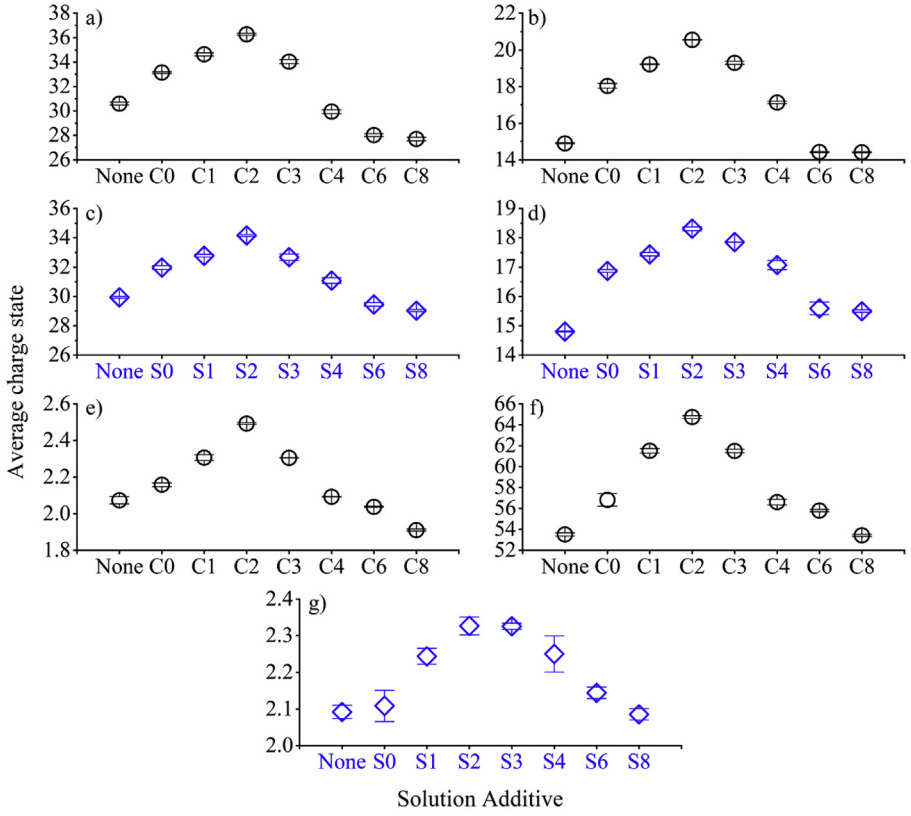

Fig. 3. Average charge states of protonated a) carbonic anhydrase II obtained with additives **C0-C8**, b) cytochrome *c* obtained with additives **C0-C8**, c) carbonic anhydrase II obtained with additives **S0-S8**, d) cytochrome *c* obtained with additives **S0-S8**, e) [Val [5]]-angiotensin II acetate obtained with additives **C0-C8**, f) bovine serum albumin obtained with additives **C0-C8**, and g) [Val [5]]-angiotensin II acetate obtained with additives **S0-S8**. Additives are listed from left to right on the x-axis in order of increasing alkyl chain length. Average charge states were obtained using ESI-MS with denaturing solutions (~80/19/1% methanol/water/acetic acid) and contained the 'optimal' concentration of each additive (refer to Table 1 and Table S7 in the Supplementary Information for tabulated data).

0.5 kJ mol^{-1} and 2 kJ mol^{-1}, respectively (see Supplementary Information Tables S6, S10, and S11). Solution-phase pK_a values of the conjugate acids of additives **C0-C8** and **S0-S8** were calculated using G3(MP2)-CC [51]//M06−2X/6-31G(d) [52] and the SM8[57] model (Supplementary Information Table S6). The dipole moments, gas-phase basicity values, and aqueous solution-phase pK_a values are presented in Fig. 4a, b, and c, respectively. For tabulated data refer to the Supplementary Information (Tables S6, S8-11).

The dipole moments and gas-phase basicity values increase marginally as the side chain lengths of the additives increase (Fig. 4a and b). From additives **C2** to **C8** and **S2** to **S8** the dipole moments and gas-phase basicity values both increase by less than 3% as the side chain lengths increase. However, the extent of protein charging decreases by up to 30% from additive **C2** to **C8** and 15% from additive **S2** to **S8**. Furthermore, the decrease in protein charging does not correlate with the increase in dipole moments and gas-phase basicity values from additives **C2** to **C8** and **S2** to **S8**. Similarly, the pK_a values of the conjugate acids of additives **C0-C8** and **S0-S8** ranged from −14.4 to −13.9 and from −18.0 to −17.3, respectively (Fig. 4c), which indicates that the Brønsted basicities of the additives are not significantly impacted by the alkyl chain length, whereas the extent of protein charging depends strongly on the chain length. Thus, these data indicate that the dipole moments, gas-phase basicity values, and Brønsted basicities of the additives are not responsible for the trends in protein charging with alkyl chain length that is observed in the ESI-MS experiments in this study (Fig. 3). However, these data cannot rule out that such properties can in principle impact the absolute extent of ion charging (*e.g.* by changing the polar head group).

Additionally, the results of circular dichroism measurements (Fig. 4d) using the same solution compositions for **C0-C8** as in the ESI experiments indicate that the chain lengths of the additives do not significantly affect the relative extent that the solution-phase structures of cytochrome *c* is disordered (60−63%); *i.e.* the proteins in the ESI solutions are largely denatured and the extent of denaturation is not significantly affected by the identity of the supercharging additives under these conditions.

The surface tensions of additives **C2-C8** and **S0-S8** have not been measured and reported in the literature. Thus, we obtained the surface tensions of additives **C2-C8** and **S0-S8** using pendant drop tensiometry experiments [50]. To obtain surface tension values using pendant drop tensiometry [50], the densities of the additives are required. As experimental data on the densities of the new additives were limited, the densities of all additives (except for **C0**) were measured using an oscillating U-tube sensor (Supplementary Information Table S1). The measured surface tensions of **C0-C8** and **S0-S8** are shown in Fig. 5.

The surface tension of additive **C1** ($\gamma = 41.5 \pm 0.5$ mN m^{-1}) is in good agreement with values from the literature, which were determined by the sessile drop technique ($\gamma = 40.9$ mN m^{-1}) [72]. The surface tensions of the additives decreased by a total of 14 mN m^{-1} (approximately 25% and 35% for **C0-C8** and **S0-S8**, respectively) as the length of the alkyl chain increased. Overall, the carbonate additives have significantly higher surface tensions than the sulphite additives with the same chain length, which may result in the formation of higher charge states using **C0-C8** than **S0-S8** (Fig. 3).

By replacing the carbonate functional group with the sulphite

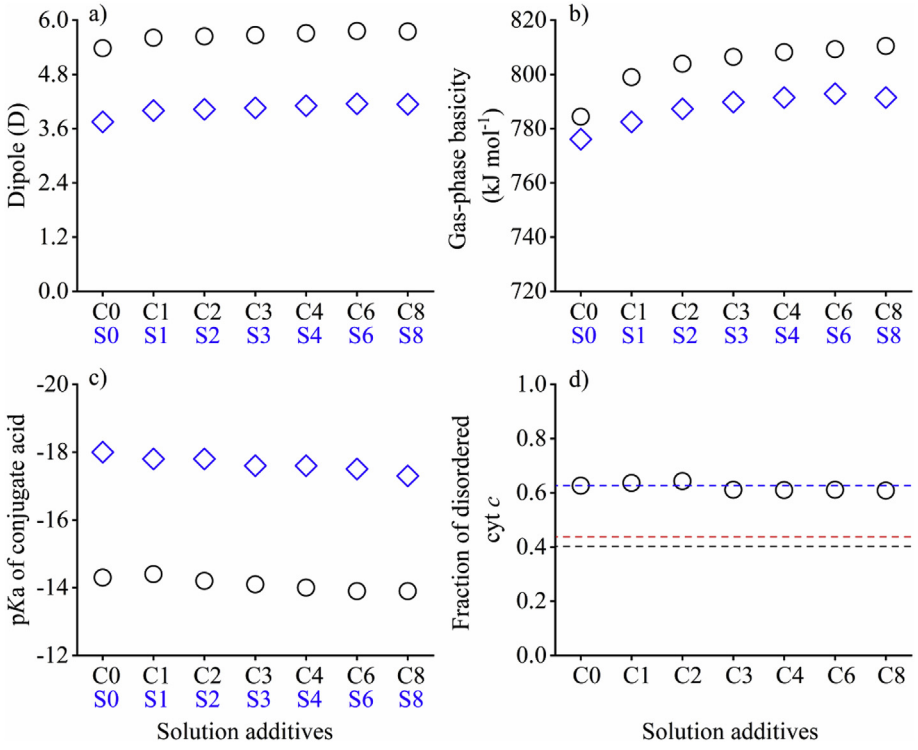

Fig. 4. a) Calculated electric dipole moments of additives **C0-C8** (open circles) and **S0-S8** (open diamonds), b) calculated gas-phase basicity values of additives **C0-C8** (open circles) and **S0-S8** (open diamonds), c) calculated pK_a values of the conjugate acids of additives **C0-C8** (open circles) and **S0-S8** (open diamonds) in water, and d) fraction of the structure of cytochrome *c* that is disordered in the ESI solutions with additives **C0-C8** (~80/19/1% methanol/water/acetic acid with "optimal" concentration of additives) obtained from circular dichroism measurements; the black, red, and blue dotted lines indicate the fraction of disordered structure in water with 1 mM ammonium acetate, in pure water, and in 80/19/1% methanol/water/acetic acid, respectively. The additives are listed on the x-axis from left to right in order of increasing alkyl chain length. Based on benchmarking calculations (Figs. S4–5), the uncertainties in the calculated gas-phase basicities of **C0-C8** and **S0-S8** are estimated to be within ~2 kJ mol^{-1} and ~10 kJ mol^{-1}, respectively. Similarly, the uncertainties in the calculated dipole moments of **C0-C8** and **S0-S8** are estimated to be within 0.1 D and 0.2 D, respectively. For tabulated data and details on the calculations, refer to Table S6 and S8-11 in the Supplementary Information.

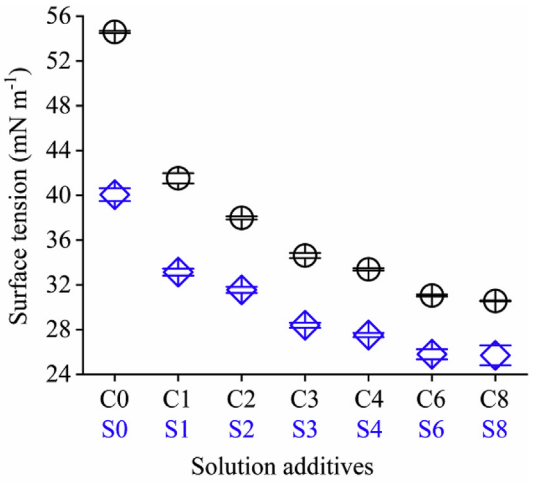

Fig. 5. Surface tensions of additives **C1**-**C8** (open circles) and **S0**-**S8** (open diamonds) measured by pendant drop tensiometry [50]. The surface tension of **C0** presented here is a value determined by Naejus et al. at 40 °C, as **C0** is a solid at room temperature [48].

functional group and keeping alkyl chain lengths constant, many properties of the additives can change. For example, the use of the sulphite polar head group compared to the carbonate group (keeping the alkyl chain length constant) results in a decrease in the surface tensions, dipole moments, gas-phase basicity values, and pK_a values of the conjugate acids by 5–15 mN m^{-1}, 1.6 D, 8–13 kJ mol^{-1}, and ~3.5 (dimensionless quantity), respectively. In addition, the use of **C0**-**C8** resulted in protein charge states (cyt *c* and CAII) that were 1–2 charge states higher than those obtained by use of **S0**-**S8** (Fig. 3). By comparing the effects of the polar head groups on the extent of ion charging (keeping the alkyl chain length constant) to the changes in the physicochemical properties between **C0**-**C8** and **S0**-**S8**, these data are in agreement with both the surface tension mechanism [29] (*i.e.* higher surface tension resulted in higher protein charge states) and the dipole moment mechanism [41] (*i.e.* larger dipole moments resulted in higher protein charge states). Although **S0**-**S8** are significantly less basic than **C0**-**C8**, higher charge states were formed by use of **C0**-**C8** than **S0**-**S8**, which is in disagreement with the Brønsted basicity mechanism [40]. Thus, the differences in average charge states achieved with additives **C0**-**C8** compared with **S0**-**S8** could be attributed to the differences in their dipole moments and surface tensions but not to the differences in their Brønsted basicities. For example, all additives are significantly less basic than water; *i.e.* the pK_a values of the conjugate acids of **C0**-**C8** and **S0**-**S8** are all significantly lower than the pK_a of H_3O^+ (−1.74) [73], which is a criterion for predicting supercharging activity for an additive using the Brønsted basicity model [40]. However, **S8** and **C8** do not exhibit any significant supercharging activity under these conditions, which is inconsistent with the Brønsted basicity model.

Almost all additives have higher surface tensions than methanol (21.8 mN m^{-1}) [74] and acetic acid (27.12 mN m^{-1}) [43] and can therefore potentially result in an increase in the surface tension of ESI generated droplets near the moment of ion formation. The precise compositions of the ESI droplets near the moment of protein ion formation are unknown. Because methanol has the lowest boiling point of all components in the analyte solution (64.5 °C) [75] it should evaporate preferentially during the ESI process [36]. Acetic acid is less volatile than water and data on binary water-acetic acid mixtures from the literature indicate that water evaporates more rapidly than acetic acid [44], so that the composition of ESI generated droplets will shift towards pure acetic acid during the ESI process. Enrichment of acetic acid should significantly lower the surface tension of largely aqueous droplets compared to pure water (72.01 mN m^{-1}) [43]. For example, at 25 °C the surface tension of a 31/69% acetic acid/water mixture is 35.79 mN m^{-1} [43], which is less than the surface tension of **C2** ($\gamma = 38.0$ mN m^{-1}, boiling point: 251 °C [76]). Thus, enrichment of the additive could increase the droplet surface tension in the final stages of ESI, particularly in the presence of high methanol and acetic acid concentrations, thus counteracting the decrease in surface tension caused by the enrichment of acetic acid.

3.3. Implications for the mechanism of supercharging

For additives **C2**-**C8** and **S2**-**S8**, the extent of protein ion charging decreases as the surface tension of the additives decreases, which is consistent with surface tension being an important factor in the supercharging mechanism for these additives. Based on Equation (1), the amount of charge a droplet of a given size can hold prior to Coulombic fission is proportional to the square root of the surface tension of the droplet. If the additives examined in this project undergo significant enrichment in concentration in ESI generated droplets owing to the preferential evaporation of solvent, the surface tension of the ESI droplets can be approximated by the surface tension of the additives. The relative amount of charge in the ESI droplets can be obtained from the protein ion charge states by assuming the extent of charge that is transferred to the protein ion in ESI is proportional to the amount of charge in the droplets. To the extent that these approximations hold and that the surface tension of the droplets limits the extent of protein charging in ESI-MS when using additives **C2**-**C8** and **S2**-**S8**, the average charge states of the tested proteins and peptides should scale approximately linearly with the square root of the surface tension of the additives.

In Fig. 6, the average charge states of cyt *c*, CAII, Ang II, and BSA are plotted *vs.* the square root of the surface tensions of additives **C2**-**C8** and **S2**-**S8**. The linear regression best fit curves to the data have R^2-values ranging from 0.818 to 0.953, with the exception of the AngII data collected using additives **S2**-**S8** ($R^2 = 0.658$). The correlation between the extent of analyte charging and additive surface tension is relatively high. Considering the approximations made above in this analysis, these data agree with the trend expected from the Rayleigh limit (Equation (1)) for protein ion charging. The decrease in the average charge states of cyt *c*, CAII, Ang II, and BSA from additives **C2** to **C8** and from **S2** to **S8** is consistent with surface tension being a limiting factor in protein supercharging for these additives; *i.e.* the extent of supercharging is limited by Coulombic fission of ESI droplets. The lower R^2-value for the AngII data obtained using additives **S2**-**S8** can be attributed in part to the relatively minor difference (~7%) in the extent of ion charging obtained for **S2** (2.31 ± 0.01) compared to **S8** (2.15 ± 0.02).

For the smaller additives (**C0**-**C2** and **S0**-**S2**), the increase in protein charge states does not correlate with an increase in additive surface tension, which suggests that a property other than surface tension can significantly impact the protein ion charging using these additives. Additionally, the use of additives **C1** and **C3** in ESI-MS resulted in similar average charge states (*e.g.* 34.6 ± 0.1 and 34.0 ± 0.2, respectively for CAII) despite additive **C3** having a surface tension that is 6.9 mN m^{-1} lower than that of additive **C1**. Similarly, the use of additives **S1** and **S3** also resulted in similar average charge states (*e.g.* 32.8 ± 0.1 and 32.7 ± 0.1, respectively for CAII) despite a difference of 4.7 mN m^{-1} in surface tension. These results suggest that a property other than surface tension is implicated in the degree of protein supercharging obtained with additives **C0**-**C2** and **S0**-**S2**.

In addition to Coulombic fission, which depends strongly on surface tension, the amount of small charge carriers in ESI

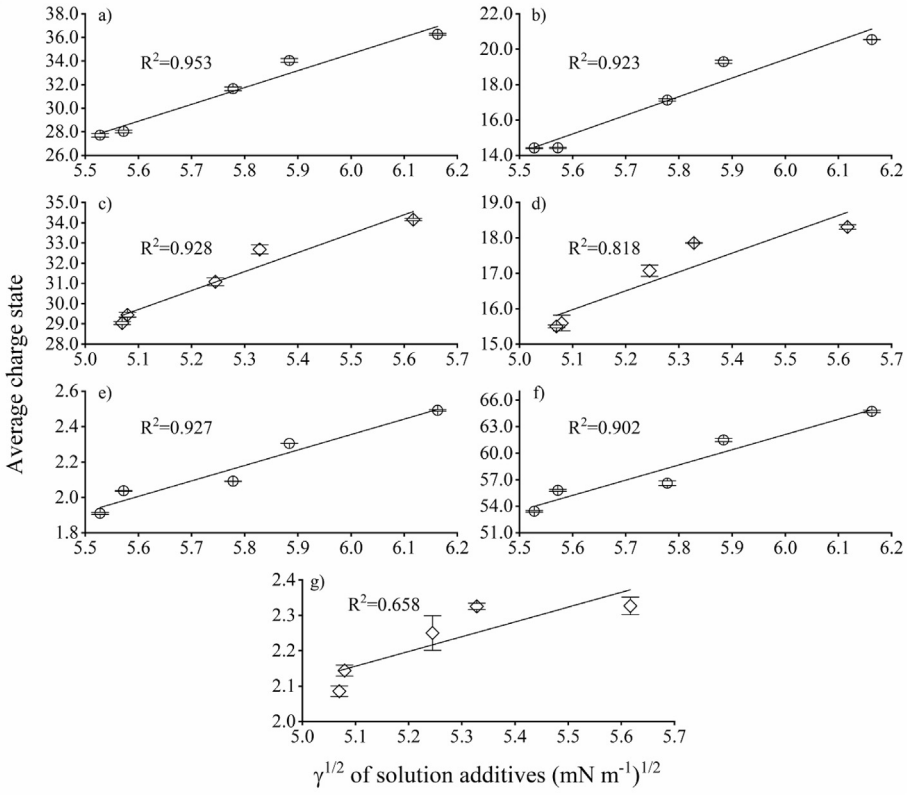

Fig. 6. Linear least squares regression fits to plots of average charge states of protonated a) carbonic anhydrase II using additives **C2-C8**, b) cytochrome *c* using additives **C2-C8**, c) carbonic anhydrase using additives **S2-S8**, d) cytochrome *c* using additives **S2-S8**, e) [Val [5]]-angiotensin II acetate using additives **C2-C8**, f) bovine serum albumin using additives **C2-C8**, and g) [Val [5]]-angiotensin II acetate using additives **S2-S8** *vs.* the square root of the surface tensions of the solution additives that were used. Average charge states were obtained using ESI-MS. ESI solutions were protein denaturing (~80/19/1% methanol/water/acetic acid) and contained an 'optimal' concentration of each additive (see Table 1 and Supplementary Information Fig. S7). Standard deviations of the square root of the surface tension of the additives were within 0.04 $(\mathrm{mN\,m^{-1}})^{1/2}$.

generated droplets (*i.e.* the charge available to be transferred to analytes) can be reduced by the emission of such charge carriers (*e.g.* H_3O^+, Na^+, and corresponding ionic hydrates) from sufficiently highly charged droplets. That is, the charge of the analyte can be limited by the emission of charge carries, in addition to Coulombic fission [28]. Unlike surface tension-limited Coulombic fission, ion emission depends primarily on the solvation energy of the charge carriers and the energy barrier associated with the loss of charge carriers from the ionic nanodroplets [28]. Thus, the emission of charge carriers from ESI-generated droplets may be the limiting process (as opposed to droplet fission) in the extent of protein charging obtained with additives **C0-C2** and **S0-S2** that have relatively high surface tensions and are relatively non-volatile.

Gross and co-workers recently reported that the charge states of globular proteins formed from droplets with similar, 'native-like' solvent compositions and different protein sizes were limited by either ion emission (for proteins < 100 kDa) or Coulombic fission (for proteins > 100 kDa) [38]. To rationalise these results, Gross and co-workers introduced the dimensionless quantity θ (Equation (3)), which is the ratio between the maximum amount of charge a droplet can hold before ion emission occurs (Q_{IE}) [38] and the maximum amount of charge a droplet can hold before Coulombic fission occurs (Q_{CF}, see Equation (1)):

$$\theta = \frac{Q_{IE}}{Q_{CF}} = E_{IE}\left(\frac{\varepsilon_0 R}{4\gamma}\right)^{\frac{1}{2}} \quad (3)$$

where ε_0 is the permittivity of vacuum, R the radius of the ESI droplet, γ the surface tension of the droplet, and E_{IE} the electric field strength required to initiate ion emission. For θ values more than 1, Coulombic fission is favoured over the emission of charge carriers and for θ values less than 1, ion emission is favoured [38]. In this formulation, θ is proportional to the square root of the droplet radius, which is consistent with the aforementioned observations made by Gross and co-workers [38]. However, in Equation (3), θ is also inversely proportional to the square root of the surface tension of the droplets; *i.e.* the use of non-volatile additives with different surface tensions should affect whether the extent of droplet charging is limited by Coulombic fission of ESI generated droplets and/or the emission of charge carriers from such droplets. In Fig. 7, a qualitative plot of the charge a droplet with 2 nm radius can accommodate as a function of surface tension is plotted for the case in which droplet charging is either Coulombic fission limited (Q_{CF}) or ion emission limited (Q_{IE}). For $Q_{IE} < Q_{CF}$ (*i.e.* when additives with high surface tensions are used), ion emission is the dominant pathway and for $Q_{CF} < Q_{IE}$ (*i.e.* when additives with low surface tensions are used), Coulombic fission is the dominant pathway for charge reduction of the ESI droplets. As Q_{IE} depends on the solvation energy of the charge carriers, *i.e.* the chemical composition of the droplets, and Q_{CF} depends on the droplets' surface tensions, both Q_{CF} and Q_{IE} should depend on the identity of the supercharging additive. The results of this study are consistent with a crossover between ion emission of charge carriers for ESI generated droplets as the dominant charge limiting mechanism for **C0-C2** and **S0-S2** (additives with relatively high surface tensions) to Coulombic fission as the dominant charge limiting pathway for **C2-C8** and **S2-S8** (additives with relatively low surface tensions). Such a crossover occurs for droplets <10 nm, which is consistent with previous

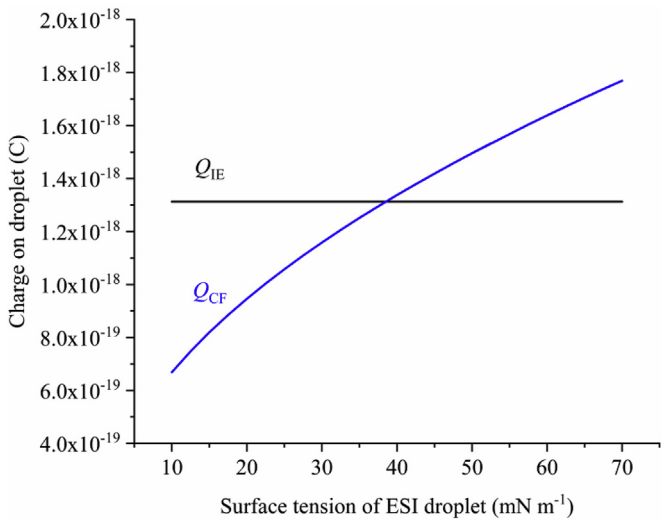

Fig. 7. Plot of the maximum charge a droplet with a 2 nm radius can hold before ion emission (Q_{IE}) and Coulombic fission (Q_{CF}) occurs as a function of surface tension of the charged droplets. Q_{CF} was calculated using Equation (1) and Q_{IE} was calculated using an equation reported by Gross and co-workers and a critical electric field strength at which ion emission occurs ($E_{IE} = 2.95\ V\ nm^{-1}$), which was determined from ESI-MS experiments on a series of globular proteins [38]. Q_{CF} depends strongly on surface tension and thus on which supercharging additive is employed. Q_{IE} does not depend on surface tension but does depend on the solvation energy of charge carriers in the ESI droplets.

molecular dynamics simulations reported in the literature [77,78] that suggest that the maximum size of droplets for ion emission and chain ejection (sequential ejection of unfolded proteins from droplets) [77,78] to occur is approximately 10 nm.

The increase in the average charge states of proteins obtained for **C0-C2** and **S0-S2** as the tail lengths of the additives increase may be related to their extent of surfactant character, which increases as the alkyl chain length increases from **C0** to **C2** and **S0** to **S2**. Based on molecular dynamics simulations, Konermann and co-workers reported that in supercharging, additives tend to form 'ionophobic' layers around the ESI droplets [79]. These results were complemented by experiments demonstrating that the addition of a crown ether (18-Crown-6) suppresses supercharging presumably by transporting ions through the ionophobic layer to the surface, which would promote the emission of ions [49]. Although these ESI-MS results were obtained using 'native-like' solution conditions, the solution composition of 'mature' ESI droplets in our study (largely water, acid, and supercharger) is expected to be similar to the composition of the ESI droplets in the study by Konermann and co-workers. An increase in the alkyl chain lengths of supercharging additives should increase the tendency of the additives to reside at the droplet surface, *i.e.* to form an ionophobic layer. Thus, the increase in alkyl chain length from **C0** and **S0** to **C2** and **S2** may result in more effective suppression of ion emission and therefore higher protein charge states. Moreover, the presence of non-ionic surfactants in water at low pH tends to result in negative surface potentials of water at the air-water interface [80–82]. As such, non-ionic surfactants such as the supercharging additives presented in this study could decrease the surface potential of the ESI droplets, which would impede the emission of positive charge carriers.

4. Conclusion

The average protein ion charge states obtained by using ESI-MS and additives **C2-C8** and **S2-S8** correlated strongly with the surface tensions of these additives. However, above a critical surface tension (*i.e.* the surface tensions of **C2** and **S2**) there was no correlation between the observed extent of protein ion charging and the surface tensions of the additives. More precisely, the increasing trend in charge states obtained with additives **C0-C2** and **S0-S2** does not correlate with their surface tensions, dipole moments, gas-phase basicity values, or Brønsted basicity, which suggests that another property (*i.e.* amphiphilicity) may be primarily responsible for the trends in protein charging observed with these additives at relatively high surface tensions. The protein ion charge states increased as the length of the side chains of additives **C0-C2** and **S0-S2** increased. The results of this study suggest that to maximise the charge states of protein ions formed by ESI-MS, solution additives with high surface tension and some amphiphilic character are desired. Furthermore, our data offers a possible explanation for the lack of correlation between the effectiveness of superchargers and their surface tensions in the data presented in the literature [32,34,47]. For superchargers with high surface tensions (*e.g. m*-NBA, **C0-C2**, **S0-S2**, etc.), properties other than surface tension (amphiphilicity) can impact the average charge states of proteins more significantly than surface tension; *i.e.* the extent of protein charging with such superchargers may be limited by the emission of charge carriers from highly charged droplets rather than droplet fission. However, the use of superchargers with relatively low surface tensions can result in the extent of protein charging being limited by droplet fission, *i.e.* limited by surface tension. The possibility of protein charging being limited by either droplet fission or the emission of charge carriers from highly charged ESI-generated droplets (Equation (3)) may explain why some studies report a correlation between surface tension [29,30,32,36] and the extent of protein charging and others do not [32,34,47]. Although a correlation between the extent of protein charging and the dipole moments, gas-phase basicity values, and Brønsted basicity of the additives was not observed, these properties cannot be ruled out as contributing factors. Future studies focusing on molecules with different dipole moments, gas-phase basicity values, and Brønsted basicities but more similar surface tension values than the additives examined in this study may provide further insights into the mechanism of supercharging and the discovery of more effective additives.

Declaration of interests

The authors declare that they have no known competing financial interests or personal relationships that could have appeared to influence the work reported in this paper.

Acknowledgements

We thank the Australian Research Council for funding. The authors acknowledge the staff of the Bioanalytical Mass Spectrometry Facility, and Dr Doug Lawes, Dr Donald Thomas, and Dr James Hook from the Nuclear Magnetic Resonance Facility in the UNSW Mark Wainwright Analytical Centre, as well as A/Prof. Graham Ball (UNSW) for helpful discussion.

Appendix A. Supplementary data

Supplementary data to this article can be found online at https://doi.org/10.1016/j.acax.2018.100004.

References

[1] J.B. Fenn, M. Mann, C.K. Meng, S.F. Wong, C.M. Whitehouse, Electrospray ionization for mass spectrometry of large biomolecules, Science (New York, N.Y.) 246 (1989) 64–71.

[2] P. Kebarle, U.H. Verkerk, Electrospray: from ions in solution to ions in the gas phase, what we know now, Mass Spectrom. Rev. 28 (2009) 898–917.
[3] N.B. Cech, C.G. Enke, Practical implications of some recent studies in electrospray ionization fundamentals, Mass Spectrom. Rev. 20 (2001) 362–387.
[4] Y.O. Tsybin, K.F. Haselmann, M.R. Emmett, C.L. Hendrickson, A.G. Marshall, Charge location directs electron capture dissociation of peptide dications, J. Am. Soc. Mass Spectrom. 17 (2006) 1704–1711.
[5] A.T. Iavarone, K. Paech, E.R. Williams, Effects of charge state and cationizing agent on the electron capture dissociation of a peptide, Anal. Chem. 76 (2004) 2231–2238.
[6] M.A. Zenaidee, W.A. Donald, Electron capture dissociation of extremely supercharged protein ions formed by electrospray ionisation, Anal. Methods 7 (2015) 7132–7139.
[7] F.W. McLafferty, D.M. Horn, K. Breuker, Y. Ge, M.A. Lewis, B. Cerda, R.A. Zubarev, B.K. Carpenter, Electron capture dissociation of gaseous multiply charged ions by fourier-transform ion cyclotron resonance, J. Am. Soc. Mass Spectrom. 12 (2001) 245–249.
[8] R.A. Zubarev, D.M. Horn, E.K. Fridriksson, N.L. Kelleher, N.A. Kruger, M.A. Lewis, B.K. Carpenter, F.W. McLafferty, Electron capture dissociation for structural characterization of multiply charged protein cations, Anal. Chem. 72 (2000) 563–573.
[9] N.L. Kelleher, H.Y. Lin, G.A. Valaskovic, D.J. Aaserud, E.K. Fridriksson, F.W. McLafferty, Top down versus bottom up protein characterization by tandem high-resolution mass spectrometry, J. Am. Chem. Soc. 121 (1999) 806–812.
[10] R.A. Zubarev, Electron-capture dissociation tandem mass spectrometry, Curr. Opin. Biotechnol. 15 (2004) 12–16.
[11] H.J. Cooper, K. Håkansson, A.G. Marshall, The role of electron capture dissociation in biomolecular analysis, Mass Spectrom. Rev. 24 (2005) 201–222.
[12] R.A. Zubarev, N.L. Kelleher, F.W. McLafferty, Electron capture dissociation of multiply charged protein cations. A nonergodic process, J. Am. Chem. Soc. 120 (1998) 3265–3266.
[13] D.M. Horn, Y. Ge, F.W. McLafferty, Activated ion electron capture dissociation for mass spectral sequencing of larger (42 kDa) proteins, Anal. Chem. 72 (2000) 4778–4784.
[14] R.A. Zubarev, K.F. Haselmann, B. Budnik, F. Kjeldsen, F. Jensen, Towards an understanding of the mechanism of electron-capture dissociation: a historical perspective and modern ideas, Eur. J. Mass Spectrom. 8 (2002) 337–349.
[15] W.A. Donald, R.D. Leib, J.T. O'Brien, A.I.S. Holm, E.R. Williams, Nanocalorimetry in mass spectrometry: a route to understanding ion and electron solvation, Proc. Natl. Acad. Sci. U. S. A 105 (2008) 18102–18107.
[16] W.A. Donald, M. Demireva, R.D. Leib, M.J. Aiken, E.R. Williams, Electron hydration and Ion–Electron pairs in water clusters containing trivalent metal ions, J. Am. Chem. Soc. 132 (2010) 4633–4640.
[17] W.A. Donald, E.R. Williams, Measuring the extent and width of internal energy deposition in ion activation using nanocalorimetry, J. Am. Soc. Mass Spectrom. 21 (2010) 615–625.
[18] W.A. Donald, E.R. Williams, Gas-phase electrochemistry: measuring absolute potentials and investigating ion and electron hydration, Pure Appl. Chem. (2011) 2129.
[19] K. Håkansson, M.J. Chalmers, J.P. Quinn, M.A. McFarland, C.L. Hendrickson, A.G. Marshall, Combined electron capture and infrared multiphoton dissociation for multistage MS/MS in a fourier transform ion cyclotron resonance mass spectrometer, Anal. Chem. 75 (2003) 3256–3262.
[20] A. Dobo, I.A. Kaltashov, Detection of multiple protein conformational ensembles in solution via deconvolution of charge-state distributions in ESI MS, Anal. Chem. 73 (2001) 4763–4773.
[21] A. Natalello, C. Santambrogio, R. Grandori, Are charge-state distributions a reliable tool describing molecular ensembles of intrinsically disordered proteins by native MS? J. Am. Soc. Mass Spectrom. 28 (2017) 21–28.
[22] K.B. Shelimov, D.E. Clemmer, R.R. Hudgins, M.F. Jarrold, Protein structure in Vacuo: gas-phase conformations of BPTI and cytochrome c, J. Am. Chem. Soc. 119 (1997) 2240–2248.
[23] S.J. Valentine, A.E. Counterman, D.E. Clemmer, Conformer-dependent proton-transfer reactions of ubiquitin ions, J. Am. Soc. Mass Spectrom. 8 (1997) 954–961.
[24] L. Konermann, D.J. Douglas, Unfolding of proteins monitored by electrospray ionization mass spectrometry: a comparison of positive and negative ion modes, J. Am. Soc. Mass Spectrom. 9 (1998) 1248–1254.
[25] R.L. Grimm, J.L. Beauchamp, Evaporation and discharge dynamics of highly charged multicomponent droplets generated by electrospray ionization, J. Phys. Chem. 114 (2010) 1411–1419.
[26] L. Rayleigh, XX. On the equilibrium of liquid conducting masses charged with electricity, Philos. Mag. A 14 (1882) 184–186.
[27] D. Duft, T. Achtzehn, R. Müller, B.A. Huber, T. Leisner, Rayleigh jets from levitated microdroplets, Nature 421 (2003), 128.
[28] J.V. Iribarne, B.A. Thomson, On the evaporation of small ions from charged droplets, J. Chem. Phys. 64 (1976) 2287–2294.
[29] A.T. Iavarone, E.R. Williams, Mechanism of charging and supercharging molecules in electrospray ionization, J. Am. Chem. Soc. 125 (2003) 2319–2327.
[30] A.T. Iavarone, J.C. Jurchen, E.R. Williams, Supercharged protein and peptide ions formed by electrospray ionization, Anal. Chem. 73 (2001) 1455–1460.
[31] C.A. Teo, W.A. Donald, Solution additives for supercharging proteins beyond the theoretical maximum proton-transfer limit in electrospray ionization mass spectrometry, Anal. Chem. 86 (2014) 4455–4462.
[32] M.A. Zenaidee, W.A. Donald, Extremely supercharged proteins in mass spectrometry: profiling the pH of electrospray generated droplets, narrowing charge state distributions, and increasing ion fragmentation, Analyst 140 (2015) 1894–1905.
[33] A.T. Iavarone, J.C. Jurchen, E.R. Williams, Effects of solvent on the maximum charge state and charge state distribution of protein ions produced by electrospray ionization, J. Am. Soc. Mass Spectrom. 11 (2000) 976–985.
[34] S.H. Lomeli, I.X. Peng, S. Yin, R.R. Ogorzalek Loo, J.A. Loo, New reagents for increasing ESI multiple charging of proteins and protein complexes, J. Am. Soc. Mass Spectrom. 21 (2010) 127–131.
[35] H.J. Sterling, J.S. Prell, C.A. Cassou, E.R. Williams, Protein conformation and supercharging with DMSO from aqueous solution, J. Am. Soc. Mass Spectrom. 22 (2011) 1178.
[36] A.T. Iavarone, E.R. Williams, Supercharging in electrospray ionization: effects on signal and charge, Int. J. Mass Spectrom. 219 (2002) 63–72.
[37] S.G. Valeja, J.D. Tipton, M.R. Emmett, A.G. Marshall, New reagents for enhanced liquid chromatographic separation and charging of intact protein ions for electrospray ionization mass spectrometry, Anal. Chem. 82 (2010) 7515–7519.
[38] C.J. Hogan, J.A. Carroll, H.W. Rohrs, P. Biswas, M.L. Gross, Combined charged residue-field emission model of macromolecular electrospray ionization, Anal. Chem. 81 (2009) 369–377.
[39] H.J. Sterling, M.P. Daly, G.K. Feld, K.L. Thoren, A.F. Kintzer, B.A. Krantz, E.R. Williams, Effects of supercharging reagents on noncovalent complex structure in electrospray ionization from aqueous solutions, J. Am. Soc. Mass Spectrom. 21 (2010) 1762–1774.
[40] R.R. Ogorzalek Loo, R. Lakshmanan, J.A. Loo, What protein charging (and supercharging) reveal about the mechanism of electrospray ionization, J. Am. Soc. Mass Spectrom. 25 (2014) 1675–1693.
[41] K.A. Douglass, A.R. Venter, Investigating the role of adducts in protein supercharging with sulfolane, J. Am. Soc. Mass Spectrom. 23 (2012) 489–497.
[42] P.D. Schnier, D.S. Gross, E.R. Williams, On the maximum charge state and proton transfer reactivity of peptide and protein ions formed by electrospray ionization, J. Am. Soc. Mass Spectrom. 6 (1995) 1086–1097.
[43] E. Álvarez, G. Vázquez, M. Sánchez-Vilas, B. Sanjurjo, J.M. Navaza, Surface tension of organic acids + water binary mixtures from 20 °C to 50 °C, J. Chem. Eng. Data 42 (1997) 957–960.
[44] K.W.M. Siu, R. Guevremont, J.C.Y. Le Blanc, R.T. O'Brien, S.S. Berman, Is droplet evaporation crucial in the mechanism of electrospray mass spectrometry? Org. Mass Spectrom. 28 (1993) 579–584.
[45] M.T. Donor, S.A. Ewing, M.A. Zenaidee, W.A. Donald, J.S. Prell, Extended protein ions are formed by the chain ejection model in chemical supercharging electrospray ionization, Anal. Chem. 89 (2017) 5107–5114.
[46] M.A. Zenaidee, M.G. Leeming, F. Zhang, T.T. Funston, W.A. Donald, Highly charged protein ions: the strongest organic acids to date, Angew. Chem. 56 (2017) 8522–8526.
[47] M. Šamalikova, I. Matečko, N. Müller, R. Grandori, Interpreting conformational effects in protein nano-ESI-MS spectra, Anal. Bioanal. Chem. 378 (2004) 1112–1123.
[48] R. Naejus, D. Lemordant, R. Coudert, P. Willmann, Excess thermodynamic properties of binary mixtures containing linear or cyclic carbonates as solvents at the temperatures 298.15 K and 315.15 K, J. Chem. Thermodyn. 29 (1997) 1503–1515.
[49] H. Metwally, L. Konermann, Crown ether effects on the location of charge carriers in electrospray droplets: implications for the mechanism of protein charging and supercharging, Anal. Chem. 90 (2018) 4126–4134.
[50] J.D. Berry, M.J. Neeson, R.R. Dagastine, D.Y.C. Chan, R.F. Tabor, Measurement of surface and interfacial tension using pendant drop tensiometry, J. Colloid Interface Sci. 454 (2015) 226–237.
[51] D.J. Henry, M.B. Sullivan, L. Radom, G3-RAD and G3X-RAD: modified Gaussian-3 (G3) and Gaussian-3X (G3X) procedures for radical thermochemistry, J. Chem. Phys. 118 (2003) 4849–4860.
[52] J.-D. Chai, M. Head-Gordon, Long-range corrected hybrid density functionals with damped atom–atom dispersion corrections, Phys. Chem. Chem. Phys. 10 (2008) 6615–6620.
[53] M.J. Frisch, G.W. Trucks, H.B. Schlegel, G.E. Scuseria, M.A. Robb, J.R. Cheeseman, G. Scalmani, V. Barone, B. Mennucci, G.A. Petersson, H. Nakatsuji, M. Caricato, X. Li, H.P. Hratchian, A.F. Izmaylov, J. Bloino, G. Zheng, J.L. Sonnenberg, M. Hada, M. Ehara, K. Toyota, R. Fukuda, J. Hasegawa, M. Ishida, T. Nakajima, Y. Honda, O. Kitao, H. Nakai, T. Vreven, J.A. Montgomery, J.E. Peralta, F. Ogliaro, M. Bearpark, J.J. Heyd, E. Brothers, K.N. Kudin, V.N. Staroverov, R. Kobayashi, J. Normand, K. Raghavachari, A. Rendell, J.C. Burant, S.S. Iyengar, J. Tomasi, M. Cossi, N. Rega, J.M. Millam, M. Klene, J.E. Knox, J.B. Cross, V. Bakken, C. Adamo, J. Jaramillo, R. Gomperts, R.E. Stratmann, O. Yazyev, A.J. Austin, R. Cammi, C. Pomelli, J.W. Ochterski, R.L. Martin, K. Morokuma, V.G. Zakrzewski, G.A. Voth, P. Salvador, J.J. Dannenberg, S. Dapprich, A.D. Daniels, Farkas, J.B. Foresman, J.V. Ortiz, J. Cioslowski, D.J. Fox, Gaussian 09, revision B.01, Gaussian, Inc., Wallingford CT, 2009.
[54] M.J. Frisch, G.W. Trucks, H.B. Schlegel, G.E. Scuseria, M.A. Robb, J.R. Cheeseman, G. Scalmani, V. Barone, G.A. Petersson, H. Nakatsuji, X. Li, M. Caricato, A.V. Marenich, J. Bloino, B.G. Janesko, R. Gomperts, B. Mennucci, H.P. Hratchian, J.V. Ortiz, A.F. Izmaylov, J.L. Sonnenberg, D. Williams-Young, F. Ding, F. Lipparini, F. Egidi, J. Goings, B. Peng, A. Petrone, T. Henderson, D. Ranasinghe, V.G. Zakrzewski, J. Gao, N. Rega, G. Zheng, W. Liang, M. Hada,

M. Ehara, K. Toyota, R. Fukuda, J. Hasegawa, M. Ishida, T. Nakajima, Y. Honda, O. Kitao, H. Nakai, T. Vreven, K. Throssell, J.A. Montgomery Jr., J.E. Peralta, F. Ogliaro, M.J. Bearpark, J.J. Heyd, E.N. Brothers, K.N. Kudin, V.N. Staroverov, T.A. Keith, R. Kobayashi, J. Normand, K. Raghavachari, A.P. Rendell, J.C. Burant, S.S. Iyengar, J. Tomasi, M. Cossi, J.M. Millam, M. Klene, C. Adamo, R. Cammi, J.W. Ochterski, R.L. Martin, K. Morokuma, O. Farkas, J.B. Foresman, D.J. Fox, Gaussian 16, revision A.03, Gaussian, Inc., Wallingford CT, 2016.

[55] Y. Shao, Z. Gan, E. Epifanovsky, A.T.B. Gilbert, M. Wormit, J. Kussmann, A.W. Lange, A. Behn, J. Deng, X. Feng, D. Ghosh, M. Goldey, P.R. Horn, L.D. Jacobson, I. Kaliman, R.Z. Khaliullin, T. Kuś, A. Landau, J. Liu, E.I. Proynov, Y.M. Rhee, R.M. Richard, M.A. Rohrdanz, R.P. Steele, E.J. Sundstrom, H.L. Woodcock, P.M. Zimmerman, D. Zuev, B. Albrecht, E. Alguire, B. Austin, G.J.O. Beran, Y.A. Bernard, E. Berquist, K. Brandhorst, K.B. Bravaya, S.T. Brown, D. Casanova, C.-M. Chang, Y. Chen, S.H. Chien, K.D. Closser, D.L. Crittenden, M. Diedenhofen, R.A. DiStasio, H. Do, A.D. Dutoi, R.G. Edgar, S. Fatehi, L. Fusti-Molnar, A. Ghysels, A. Golubeva-Zadorozhnaya, J. Gomes, M.W.D. Hanson-Heine, P.H.P. Harbach, A.W. Hauser, E.G. Hohenstein, Z.C. Holden, T.-C. Jagau, H. Ji, B. Kaduk, K. Khistyaev, J. Kim, J. Kim, R.A. King, P. Klunzinger, D. Kosenkov, T. Kowalczyk, C.M. Krauter, K.U. Lao, A.D. Laurent, K.V. Lawler, S.V. Levchenko, C.Y. Lin, F. Liu, E. Livshits, R.C. Lochan, A. Luenser, P. Manohar, S.F. Manzer, S.-P. Mao, N. Mardirossian, A.V. Marenich, S.A. Maurer, N.J. Mayhall, E. Neuscamman, C.M. Oana, R. Olivares-Amaya, D.P. O'Neill, J.A. Parkhill, T.M. Perrine, R. Peverati, A. Prociuk, D.R. Rehn, E. Rosta, N.J. Russ, S.M. Sharada, S. Sharma, D.W. Small, A. Sodt, T. Stein, D. Stück, Y.-C. Su, A.J.W. Thom, T. Tsuchimochi, V. Vanovschi, L. Vogt, O. Vydrov, T. Wang, M.A. Watson, J. Wenzel, A. White, C.F. Williams, J. Yang, S. Yeganeh, S.R. Yost, Z.-Q. You, I.Y. Zhang, X. Zhang, Y. Zhao, B.R. Brooks, G.K.L. Chan, D.M. Chipman, C.J. Cramer, W.A. Goddard, M.S. Gordon, W.J. Hehre, A. Klamt, H.F. Schaefer, M.W. Schmidt, C.D. Sherrill, D.G. Truhlar, A. Warshel, X. Xu, A. Aspuru-Guzik, R. Baer, A.T. Bell, N.A. Besley, J.-D. Chai, A. Dreuw, B.D. Dunietz, T.R. Furlani, S.R. Gwaltney, C.-P. Hsu, Y. Jung, J. Kong, D.S. Lambrecht, W. Liang, C. Ochsenfeld, V.A. Rassolov, L.V. Slipchenko, J.E. Subotnik, T. Van Voorhis, J.M. Herbert, A.I. Krylov, P.M.W. Gill, M. Head-Gordon, Advances in molecular quantum chemistry contained in the Q-Chem 4 program package, Mol. Phys. 113 (2015) 184–215.

[56] M. Valiev, E.J. Bylaska, M. Govind, K. Kowalski, T.P. Straatsma, H.J.J. van Dam, D. Wang, J. Nieplocha, E. Apra, T.L. Windus, W.A. de Jong, NWChem: a comprehensive and scalable open-source solution for large scale molecular simulations, Comput. Phys. Commun. 181 (2010) 1477.

[57] A.V. Marenich, R.M. Olson, C.P. Kelly, C.J. Cramer, D.G. Truhlar, Self-consistent reaction field model for aqueous and nonaqueous solutions based on accurate polarized partial charges, J. Chem. Theor. Comput. 3 (2007) 2011–2033.

[58] O. Sackur, Die Anwendung der kinetischen Theorie der Gase auf chemische Probleme, Ann. Phys. 341 (1911) 958–980.

[59] M.D. Tissandier, K.A. Cowen, W.Y. Feng, E. Gundlach, M.H. Cohen, A.D. Earhart, J.V. Coe, T.R. Tuttle Jr., The proton's absolute aqueous enthalpy and gibbs free energy of solvation from cluster-ion solvation data, J. Phys. Chem. 102 (1998) 7787–7794.

[60] C.P. Kelly, C.J. Cramer, D.G. Truhlar, Aqueous solvation free Energies of ions and ion-water clusters based on an accurate value for the absolute aqueous solvation free energy of the proton, J. Phys. Chem. B 110 (2006) 16066–16081.

[61] J. Ho, M.L. Coote, A universal approach to continuum solvent pKa calculations - are we there yet? Theor. Chem. Acc. 125 (2010) 3–21.

[62] J. Ho, M.L. Coote, First-principles prediction of acidities in the gas and solution phase, Wiley Interdiscip. Rev. Comput. Mol. Sci. 1 (2011) 649–660.

[63] W.A. Donald, E.R. Williams, An improved cluster pair correlation method for obtaining the absolute proton hydration energy and enthalpy evaluated with an expanded data set, J. Phys. Chem. B 114 (2010) 13189–13200.

[64] W.A. Donald, R.D. Leib, J.T. O'Brien, M.F. Bush, E.R. Williams, Absolute standard hydrogen electrode potential measured by reduction of aqueous nanodrops in the gas phase, J. Am. Chem. Soc. 130 (2008) 3371–3381.

[65] W.A. Donald, R.D. Leib, M. Demireva, J.T. O'Brien, J.S. Prell, E.R. Williams, Directly relating reduction energies of gaseous Eu(H2O)n3+, n = 55–140, to aqueous solution: the absolute SHE potential and real proton solvation energy, J. Am. Chem. Soc. 131 (2009) 13328–13337.

[66] W.A. Donald, R.D. Leib, J.T. O'Brien, E.R. Williams, Directly relating gas-phase cluster measurements to solution-phase hydrolysis, the absolute standard hydrogen electrode potential, and the absolute proton solvation energy, Chem. Eur J. 15 (2009) 5926–5934.

[67] J.-W. Huang, M. Shi, Chemical fixation of carbon dioxide by NaI/PPh3/PhOH, J. Org. Chem. 68 (2003) 6705–6709.

[68] C. Marti, E.M. Carreira, Total synthesis of (−)-Spirotryprostatin B: synthesis and related studies, J. Am. Chem. Soc. 127 (2005) 11505–11515.

[69] A.L. Hickey, C.N. Rowley, Benchmarking quantum chemical methods for the calculation of molecular dipole moments and polarizabilities, J. Phys. Chem. 118 (2014) 3678–3687.

[70] W. Sun, G.R. Kinsel, D.S. Marynick, Computational estimates of the gas-phase basicity and proton affinity of glutamic acid, J. Phys. Chem. 103 (1999) 4113–4117.

[71] F.H. Yassin, D.S. Marynick, Computational estimates of the gas-phase basicities, proton affinities and ionization potentials of the six isomers of dihydroxybenzoic acid, Mol. Phys. 103 (2005) 183–189.

[72] J. Maldonado-Valderrama, M. Cabrerizo-Vílchez, A. Bateni, M. Cabezas, R. David, A. Neumann, Applied Surface Thermodynamics, second ed., CRC Press, 2010, pp. 205–281.

[73] C. Laurence, J.-F. Gal, Lewis Basicity and Affinity Scales, Wiley, Chichester, 2010.

[74] S. Nath, Surface tension of nonideal binary liquid mixtures as a function of composition, J. Colloid Interface Sci. 209 (1999) 116–122.

[75] H. Zhu, Q. Cao, C. Li, X. Mu, Acidic resin-catalysed conversion of fructose into furan derivatives in low boiling point solvents, Carbohydr. Res. 346 (2011) 2016–2018.

[76] A. Behr, P. Bahke, B. Klinger, M. Becker, Application of carbonate solvents in the telomerisation of butadiene with carbon dioxide, J. Mol. Catal. Chem. 267 (2007) 149–156.

[77] L. Konermann, E. Ahadi, A.D. Rodriguez, S. Vahidi, Unraveling the mechanism of electrospray ionization, Anal. Chem. 85 (2013) 2–9.

[78] L. Konermann, A.D. Rodriguez, J. Liu, On the formation of highly charged gaseous ions from unfolded proteins by electrospray ionization, Anal. Chem. 84 (2012) 6798–6804.

[79] H. Metwally, R.G. McAllister, V. Popa, L. Konermann, Mechanism of protein supercharging by sulfolane and m-nitrobenzyl alcohol: molecular dynamics simulations of the electrospray process, Anal. Chem. 88 (2016) 5345–5354.

[80] R.-H. Yoon, J.L. Yordan, Zeta-potential measurements on microbubbles generated using various surfactants, J. Colloid Interface Sci. 113 (1986) 430–438.

[81] J.A. McShea, I.C. Callaghan, Electrokinetic potentials at the gas-aqueous interface by spinning cylinder electrophoresis, Colloid Polym. Sci. 261 (1983) 757–766.

[82] S. Usui, H. Sasaki, Zeta potential measurements of bubbles in aqueous surfactant solutions, J. Colloid Interface Sci. 65 (1978) 36–45.